Superior Colliculus-Projected GABAergic Retinal Ganglion Cells Mediate Looming-Evoked Flight Response

Xue Luo[1]*, Danrui Cai[1]*, Kejiong Shen[1], Qinqin Deng[1], Xinlan Lei[1], Sen Jin[2], Wen-Bo Zeng[3], Hua Li[4], Fuqiang Xu[5,6], Lu Huang[7,8], Chaoran Ren[8,9], Min-Hua Luo[3], Ting Xie[4, 10#], Yin Shen[1,11#]

[1]Eye center, Renmin Hospital of Wuhan University, Wuhan, 430060, Hubei, China

[2]HUST-Suzhou Institute for Brainsmatics, JITRI Institute for Brainsmatics, Suzhou 215125, China

[3]State Key Laboratory of Virology, CAS Center for Excellence in Brain Science and Intelligence Technology (CEBSIT), Wuhan Institute of Virology, Chinese Academy of Sciences, Wuhan 430071, China

[4]Stowers Institute for Medical Research, 1000 East 50th Street, Kansas City, MO 64110, USA

[5]Brain Cognition and Brain Disease Institute (BCBDI), Shenzhen Institutes of Advanced Technology, Chinese Academy of Sciences, Shenzhen-Hong Kong Institute of Brain Science-Shenzhen Fundamental Research Institutions, Shenzhen 518055, China

[6]Centre for Brain Science, State Key Laboratory of Magnetic Resonance and Atomic Molecular Physics, Key Laboratory of Magnetic Resonance in Biological Systems, Wuhan Institute of Physics and Mathematics, CAS Centre for Excellence in Brain Science and Intelligence Technology, Chinese Academy of Sciences, Wuhan 430071, China

[7]Department of Neurology and Stroke Center, The First Affiliated Hospital of Jinan University, Guangzhou 510632, China

[8]Guangdong-Hongkong-Macau Institute of CNS Regeneration, Ministry of Education CNS Regeneration Collaborative Joint Laboratory, Jinan University, Guangzhou 510632, China

[9]Guangzhou Regenerative Medicine and Health Guangdong Laboratory, Guangzhou 510530, China

[10]Department of Anatomy and Cell Biology, University of Kansas School of Medicine, 3901 Rainbow Blvd, Kansas City, KS 66160, USA

[11]Medical Research Institute, Wuhan University, Wuhan, 430071, China

*These authors contributed equally

[#]Correspondence:

Yin Shen, yinshen@whu.edu.cn. Eye center, Wuhan University Renmin Hospital, Medical Research Institute, Wuhan University, Wuhan, 430060, Hubei, China

Ting Xie, tgx@stowers.org. Department of Anatomy and Cell Biology, University of Kansas School of Medicine, 3901 Rainbow Blvd, and Stowers Institute for Medical Research, 1000 East 50th Street, Kansas City, MO 64110, USA

Grant support:

This work was supported by grants from the National Key R&D Program of China (2017YFE013400 to Y.S.), the National Nature Science Foundation of China (81470628 Y. S. 81800872 to Q.D.) and The Stowers SIMR fund (to T. X.).

Running title: spgRGCs mediate innate fear response

Key words: spgRGCs, innate defensive behavior, GABA, looming, superior colliculus, flight response

Abstract

The looming stimulus-evoked flight response is an experimental paradigm for studying innate defensive behaviors. However, how the visual looming stimulus is transmitted from the retina to the brain remains poorly understood. Here, we report that superior colliculus (SC)-projected GABAergic RGCs (spgRGCs) transmit the looming signal from the retina to the brain to mediate the looming-evoked flight behavior by releasing GABA. In the mouse retina, GABAergic RGCs are capable of projecting to many brain areas, including the SC. spgRGCs are mono-synaptically connected to the parvalbumin-positive SC neurons known to be required for the looming-evoked flight response. Optogenetic activation of spgRGCs triggers GABAergic responses in SC neurons. The ablation or silence of spgRGCs compromises looming-evoked flight response but not image-forming functions. Therefore, this study shows that spgRGCs control the looming-evoked flight response by regulating SC neurons via GABA, providing novel insight into the regulation of innate defensive behaviors.

Introduction

The ability to detect the naturally occurring looming stimulus, which mimics approaching objects, is a conserved innate defensive behavior important for the survival of animal species, ranging from *Drosophila* to mammals, including humans (Ball & Tronick, 1971; Gibson et al., 2015; Schiff, Caviness, & Gibson, 1962). The looming stimulus-induced flight response in mice has been recently established as an effective model for studying innate defensive behaviors in animals (L. Huang et al., 2017; Shang et al., 2015; Yilmaz & Meister, 2013). The neural circuits for mediating the looming-evoked innate defensive behavior in the mouse brain have recently been shown to involve different brain areas, including the superior colliculus (SC). However, how the looming stimulus signal is transmitted from the retina to the brain remains largely elusive.

The looming-evoked innate defensive behavior has recently been shown to involve the brain neural circuits mediated through the SC, the parabigeminal nucleus (PBGN), lateral posterior thalamic nucleus (LPTN), the ventral tegmental area (VTA), the zona incerta (ZI) and the amygdala in the mouse. The SC is generally believed to serve as a sensory-motor center for processing and controlling innate visual behaviors (Ito & Feldheim, 2018; Zhao, Liu, & Cang, 2014). Parvalbumin positive (PV^+) glutamatergic excitatory neurons in the superficial layer of the SC project to different brain areas to mediate the looming-evoked escape and freezing behavior (Shang et al., 2015). Interestingly, the looming stimulus simultaneously activate two distinct groups of PV^+ GABAergic SC neurons projecting the

PBGN and the LPTN, which both innervate the amygdala where the fear response is initiated, to mediate escape and freezing responses, respectively (Shang et al., 2019). Also, glutamatergic SC neurons innervate and send excitatory signals to GABAergic neurons in the VTA, which further project to the central nucleus of the amygdala, mediating the looming-evoked defensive behavior (Zhou et al., 2019). Although GABAergic neurons in the ZI directly innervate excitatory neurons in the dorsolateral and ventrolateral compartments of periaqueductal gray (PAG) to drive escape and freezing responses, it remains unclear how these neurons are connected to the SC (Chou et al., 2018).

The visual looming stimulus must be transmitted through retinal ganglion cells (RGCs) since they are the only cell type connecting the eye to the brain. Interestingly, GABAergic DRN neurons antagonize the serotonergic DRN neurons to activate the SC-LPTN-amygdala pathway to mediate the looming-evoked flight response (L. Huang et al., 2017). It still remains unclear how the SC/DRN-projected RGCs transmit the looming stimulus signal. Here we identified SC-projected GABAergic RGCs (spgRGCs) transmit the looming stimulus signal and mediate the looming-evoked flight response by releasing GABA.

Results

The mouse retina contains a population of GABAergic RGCs projecting to different regions of the brain

Earlier studies suggest the existence of GABA-immunoreactive RGCs in turtle (Hurd & Eldred, 1989) and rabbit retinas (Yu, Watt, Lam, & Fry, 1988)·(Hirano, Brandstatter, & Brecha, 2005), but their biological functions remain undefined. To confirm the existence of GABAergic RGCs in the mouse retina, the recombinant adeno-associated virus (AAV) expressing EYFP-EYFP in a Cre-dependent manner were injected into the vitreous of adult eyes of *Gad2-Cre* or *vGAT-Cre* mice, which are specifically expressed in GABAergic neurons (Chan et al., 2017; Fang, Yamaguchi, Song, Tritsch, & Lin, 2018; Garcia-Junco-Clemente et al., 2017; Milstein et al., 2015; Taniguchi et al., 2011) (Fig. 1A). In addition to EYFP-labeled GABAergic amacrine cells in the inner nuclear layer (INL), EYFP-labeled GABAergic RGCs in the ganglion cell layer (GCL) also existed based on their EYFP-positive optic nerve and laminar positions (Baden et al., 2016; Pang & Wu, 2011; Zhang, Kolodkin, Wong, & James, 2017) (Fig. 1B). Those EYFP-labeled RGCs were not caused by virus leakage since there were no EYFP-labeled retinal cells in negative controls (Fig. S1). Consistently, 13% of RGCs (n=6225) are positive for *Gad2* mRNA expression based on the previously published scRNA results (Rheaume et al., 2018) (Fig. 1C). Interestingly, *Gad2* mRNA is expressed in most of the identified 40 RGC subpopulations, ranging from 4% to 30%. Those labeled YFP-labeled GABAergic RGCs project their axons in the optic track (Opt) in the brain, and mainly innervate the suprachiasmatic nucleus (SCN), the lateral

112 geniculate nucleus (LGN) and the SC, but not the dorsal raphe nucleus (DRN) (Fig. 1D-H). In
113 the LGN, the axonal arbors of the GABAergic RGCs spread across the LGN, but appear to be
114 more abundant in the dorsal side (DLG) and intergeniculate leaflet (ILG) than in the ventral
115 side (VLG) (Fig. 1F). In the SC, the axonal arbors of GABAergic RGCs are more restricted to
116 the superficial and intermediate layers (SL and IL) in the SC (Fig. 1G). Taken together,
117 GABAergic RGCs exist in the adult mouse eye and are capable of projecting to the brain
118 areas participating in image-forming and non-image-forming functions.

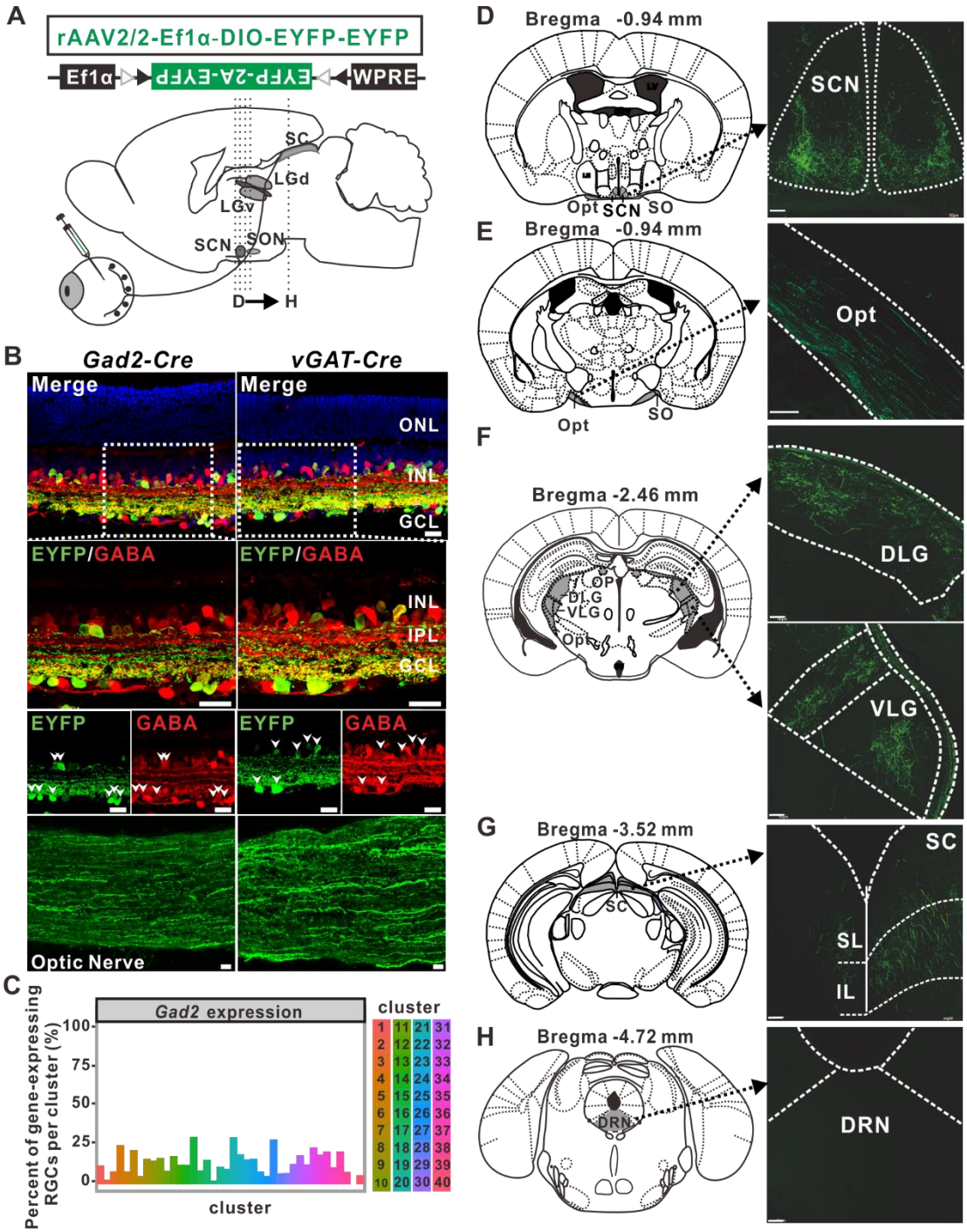

119 **Figure 1.** GABAergic RGCs project to multiple areas of the mouse brain**.** (**A**) Schematic

120 diagrams explaining the anterograde labeling of GABAergic RGCs and the gene structure for

121 Cre-dependent expression of two copies of EYFP in the AAV. (**B**) EYFP-labeled GABAergic

122 neurons in the *Gad2-Cre* (left) and *vGAT-Cre* (right) retinas. EYFP-labeled RGCs are

expressing gamma-aminobutyric acid (GABA) (shown in high magnifications, 100X), and can also extend EYFP-positive axons in the optic nerve (ONL: outer nuclear layer; INL: inner nuclear layer; GCL: ganglion cell layer; Scale bar: 20 μm). (**C**) *Gad2* mRNA expression in mouse RGC subpopulations based on the previously published scRNA results. (**D**-**H**) Brain projections from the EYFP-labeled RGCs revealed by anterograde labeling. These retinorecipient brain regions (shown in high magnifications; right) correspond to the green-filled areas in the mouse brain atlas (left) (SCN: suprachiasmatic nucleus; Opt: optic tract; SC: superior colliculus; DLG: dorsal lateral geniculate nucleus; IGL: intergeniculate leaf; VLG: ventral lateral geniculate nucleus; DRN: dorsal raphe nucleus. Scale bar: 100 μm).

spgRGCs are capable of releasing GABA to elicit physiological responses in SC neurons

To determine if spgRGCs can functionaly release GABA to elicit post-synaptic responses in SC neurons, channel Rhodopsin 2 and EYFP fusion protein (ChR2-EYFP) were expressed in the AAV-infected GABAergic RGCs. When spgRGCs were activated by 470 nm laser light, post-synaptic SC responses were recorded (Fig. 2A and 2B). Brief pulses of light can induce sustained inward currents in the ChR2-EYFP-expressing RGCs, indicating that ChR2-EYFP can be functional in GABAergic RGCs (Fig. 2C). In the SC, light-mediated ChR2 activation in the ChR2-EYFP-expressing RGC axonal fibers induces inhibitory postsynaptic currents (IPSCs) when $V_{holding}$ was set to 0 mV, which is close to the reversal potential for Na^+ (Mitamura, Higashiyama, Taniguchi, Klagsbrun, & Mekada, 1995) (Fig. 2D and 2E). The addition of bicuculline (10 μM), $GABA_A$ receptor antagonist, to the recording

143 bath solution (TTX+D-AP5+ CNQX） could reversibly suppress the light-evoked responses
144 (n=26; 21.7±4.2 pA) (Fig. 2E). To further characterize the properties of CHR2-induced
145 currents, in the all recording neurons, we also found ChR2-evoked excitatory (−70 mV) and
146 inhibitory (0 mV) currents in some postsynaptic neurons (n=14) in the presence of TTX (Fig.
147 S2). Our findings indicate that spgRGCs innervate and functionally inhibit SC neurons
148 through releasing GABA.

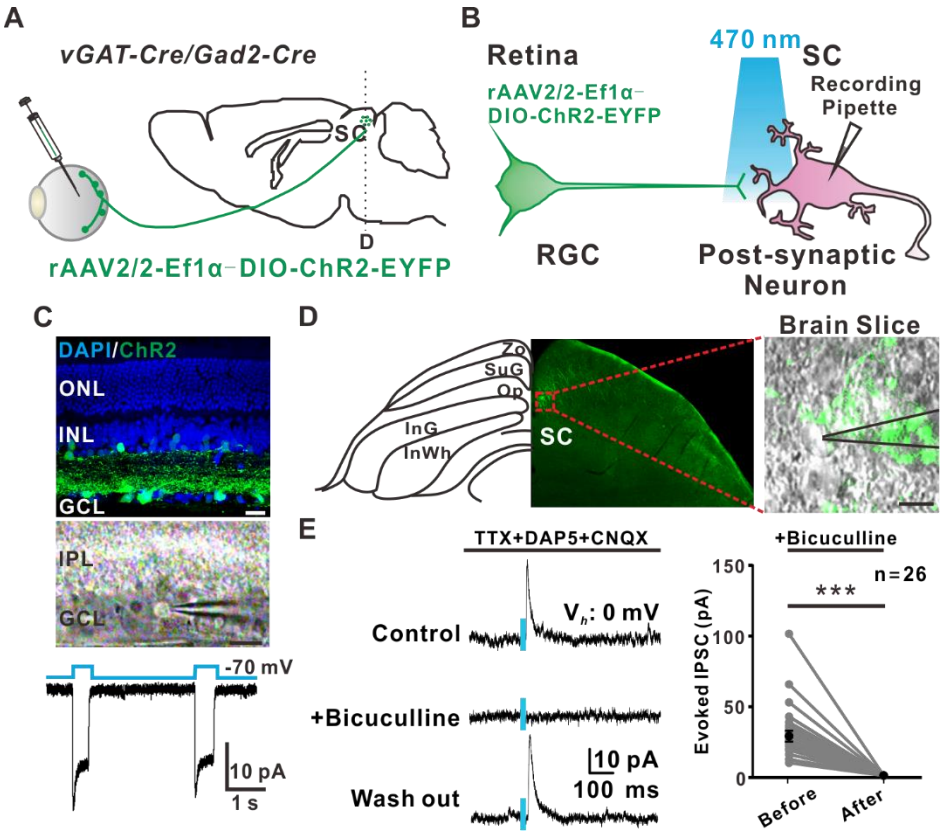

149 **Figure 2.** ChR2-mediated activation causes GABAergic RGCs to release GABA and evoke
150 electrophysiological responses in SC neurons. (**A**, **B**) Schematic representation of optogenetic
151 stimulation of GABAergic RGCs and recordings in labelled RGCs and SC neurons in tissue
152 slices. (**C**) Patch-clamp recording of the AAV-ChR2-EYFP infected RGCs in the *vGAT-*
153 *Cre*/*Gad2-Cre* retina. Light stimulation of ChR2 (470 nm, 500 ms) induces typical inward
154 currents in the ChR2-EYFP-expressing RGCs. Scale bar: 25 μm. (**D**) Recording of an RGC-

projecting SC neuron following light-induced activation of EYFP-expressing axonal fibers (green) of GABAergic RGCs (scale bar: 10 μm). (**E**) Postsynaptic IPSCs of a GABAergic RGC-projecting SC neuron in response to ChR2-mediated activation of RGCs (470nm blue light for 5 ms) are reversibly inhibited by $GABA_A$ receptor antagonist Bicuculline (10 μM). All recordings are performed with the 0 mV holding potential ($V_{holding}$) in the presence of D-AP5, strychnine, CNQX and TTX. Right: quantification results on IPSCs. Light stimulation (470 nm) is marked by a blue bar. Statistical analysis: one-way Student's t-test; ***: $P<$ 0.001.

spgRGCs are composed of ON, OFF and ON-OFF types

To further characterize the distribution, dendritic morphology and light responses of the spgRGCs, Cre-dependent EYFP-EYFP-expressing AAV viruses were injected into the SC region of the *vGAT-Cre* or *Gad2-Cre* brain for retrogradely labeling spgRGCs (Fig. 3A and 3B). Retrogradely labeled RGCs are GABAergic since the EYFP-labeled RGCs express GABA (n=12 mice) (Fig. 3C). By comparing to the Brn3a-positive ($Brn3a^+$) RGCs, which are more dense in the central retina than in the peripheral retina (O'Sullivan et al., 2017), the EYFP-labeled spgRGCs showed a higher density in the peripheral retina than in the central retina (Fig. 3D-F). 74% of EYFP-labeled spgRGCs had the soma diameter smaller than 12.5 μm, which was considered to be a small RGC soma (Sun, Li, & He, 2002). Based on stratification patterns and light-induced responses, RGCs are classified into ON, OFF, and ON-OFF subtypes. spgRGCs can also be assigned into ON, OFF, and ON-OFF subtypes

(Sernagor, Eglen, & Wong, 2001) (ON cells: n=5; OFF cells: n=3; ON-OFF cells: n=4) based on stratification and induced-response pattern (Fig. 3I-K). Thus, spgRGCs have different subtypes and exhibit a preferential periphery distribution in the retina.

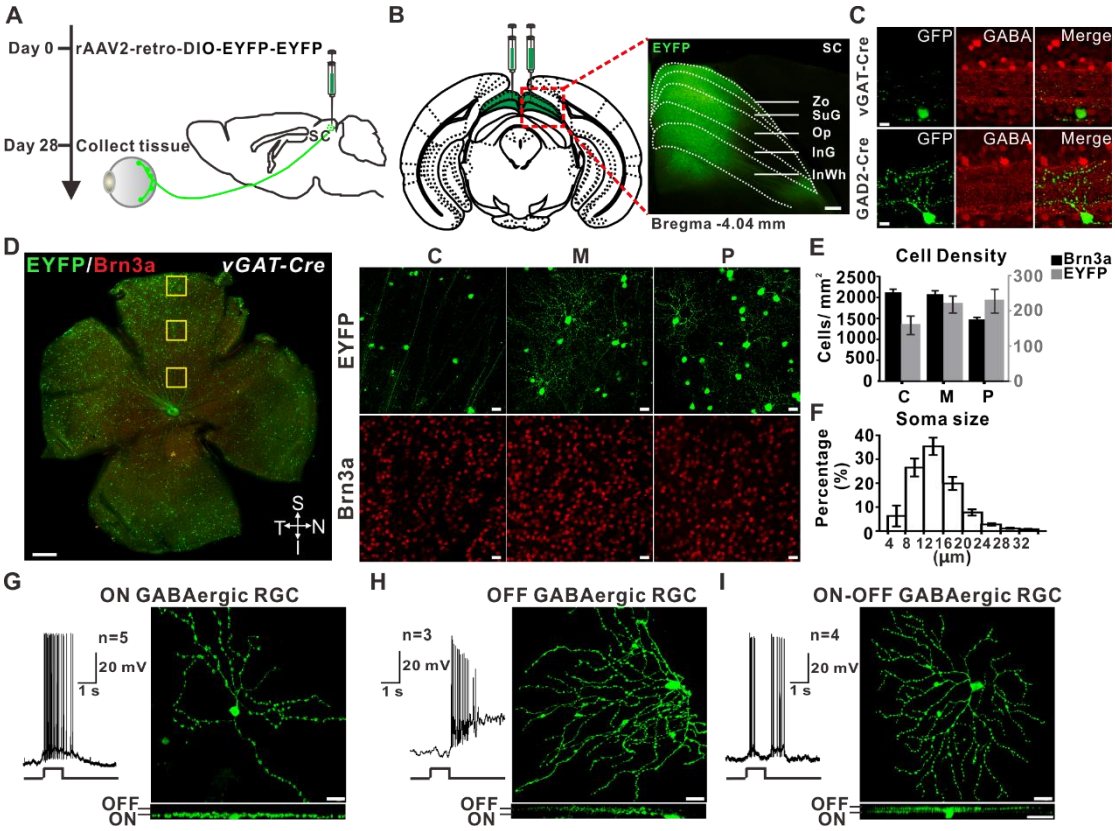

Figure 3. Morphological and functional characterization of spgRGCs. (**A**, **B**) Experimental design: *AAV-EF1a::DIO-EYFP-EYFP* viruses are delivered into the SC to retrogradely trace spgRGCs. Scale bar: 200 μm. (**C**) EYFP-labeled RGCs also express GABA. Scale bar: 200 μm. (**D**) Representative images of the distribution of EYFP (**upper**) or Brn3a (**lower**) positive RGCs in the flat mount retina of *vGAT-Cre* mice (C: Center; M: Midperiphery; P: Periphery). Highly magnified regions (40X, Scale bar: 500 μm) are shown in the right. (**E**) Retinal distributions of the SC-projected GABAergic RGCs versus Brn3a$^+$ RGCs (n=24; means ± SEM). (**F**) Histogram showing the soma size distribution of the SC-projected GABAergic

RGCs. (**G**-**I**) Light responses and dendritic morphologies of the SC-projected ON (**G**), OFF (**H**) and ON-OFF (**I**) GABAergic RGCs. Top: flat view; bottom: side view. Scale bar: 20 μm.

spgRGCs mediate the looming-evoked flight response

To further determine the downstream neurons of spgRGC-projecting SC neurons, we injected the herpes simplex virus (HSV) expressing double-floxed four copies of tandemly repeated GFP genes (HSV-LSL-TK-G4) into the vitreous of *vGAT-Cre* mice to label trans-synaptic neurons (Fig. 4A). HSV-LSL-TK-G4 is still capable of identifying potential postsynaptic targets and facilitates the identification of the cell types. GFP was detected in the SC, the PBG nucleus, the DLG (the relay center in thalamus for the visual pathway) and the pontine nucleus (Pn; involved in motor activity) in the brain (Fig. 4B). In the SC, the trans-synaptically labeled SC neurons were parvalbumin-positive (PV^+) (Fig. 4B). These results indicate that spgRGCs are synaptically connected to PV^+ SC neurons, which are known to form the circuitry controlling the looming-induced flight behavior (Shang et al., 2019; Shang et al., 2015), suggesting that spgRGCs might be involved in the looming-evoked flight response.

To directly test their requirement for the looming-evoked flight behavior, we sought to selectively ablate spgRGCs by expressing diphtheria toxin subunit A (DTA), which inactivates elongation factor 2 to terminate protein synthesis and thus kill DTA-expressing cells (Collier, 2001; Mitamura et al., 1995). AAV2/2-fDIO-DTA and AAV2/retro-Ef1α -

DIO-FLP viruses were injected into the vitreous and the SC of the *vGAT-Cre* or *Gad2-Cre* mice, respectively, to simultaneously infect the EYFP-labeled spgRGCs for allowing the Cre-dependent expression of FLP that then drives FRT-dependent DTA expression specifically in spgRGCs (Fig. 4C). Two months after dual virus infection, EYFP-labeled spgRGCs have been reduced by approximately 90% (before ablation/phase 1: 204±10.68 EYFP-positive spgRGCs/mm^2, n=11; after ablation/phase 3: 25.97±2.17 EYFP-positive spgRGCs/mm^2, n=10; $P<0.001$). In the looming stimulus-induced flight behavior test (Zhao et al., 2014), there was a significant increase in both “the time to the shelter” and “the walk distance” for the mice depleting spgRGCs (Fig. 4D-G, Supplemental Movie 1-4). Moreover, the defective looming-evoked flight response caused by spgRGC ablation persists 4 months after the ablation (Fig. 4F and 4G). Consistently, the ablation of spgRGCs significantly decreased the number of looming stimulation-induced c-Fos-positive neurons in both the SC and the PBGN, further supporting that spgRGCs are required for looming-induced neuronal activities in the SC-PGBN pathway (Fig. 4H and I). c-Fos expression is indicative of neuronal activation upon looming signaling-induced stimulation. Thus, our findings indicate that spgRGCs are required for the looming-evoked flight response by activating the SC-PGBN pathway.

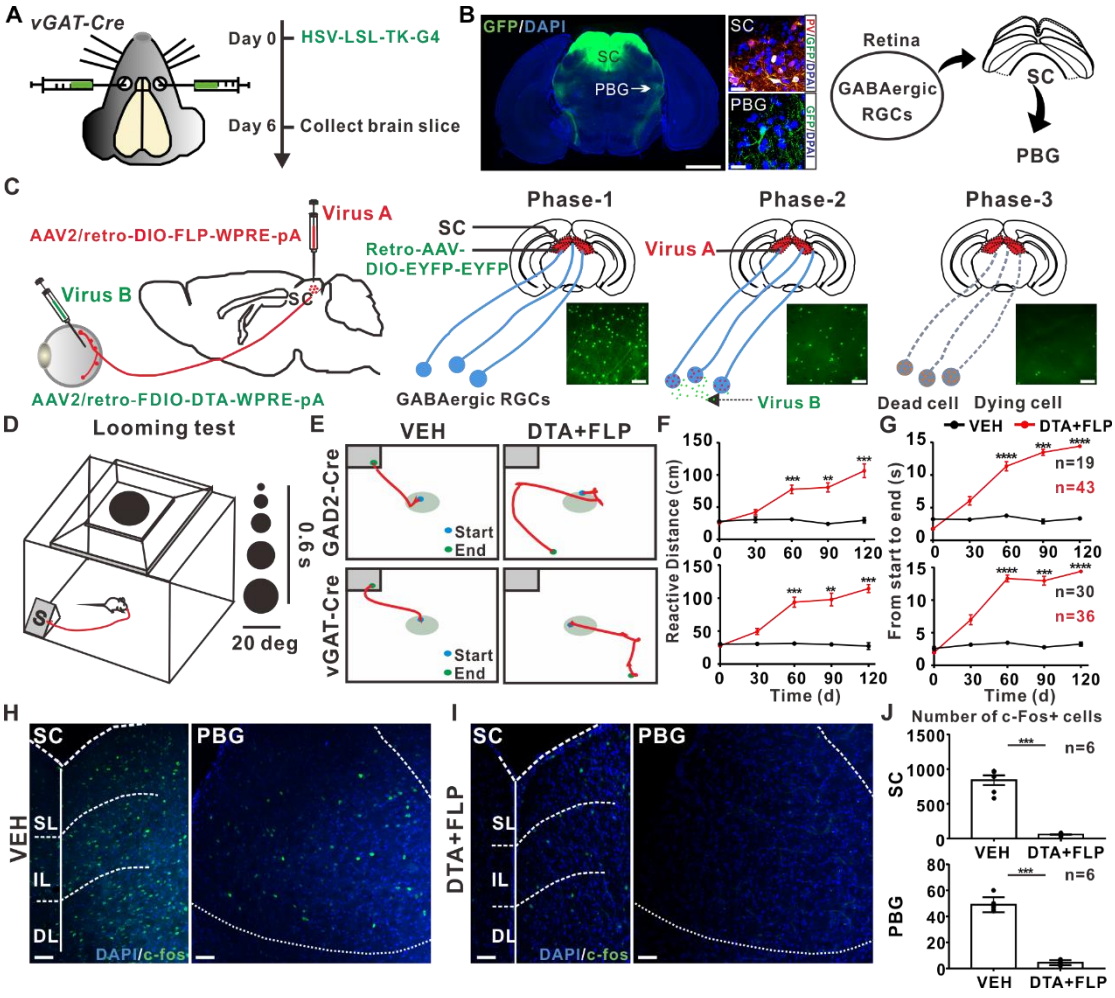

221 **Figure 4.** spgRGCs are required for the looming-evoked flight response. (**A**) Experiment
222 design for the trans-synaptic labeling of GABAergic RGCs. (**B**) By infecting the *Gad2-Cre* or
223 *vGAT-Cre* mouse eye with Cre-dependent HSV viruses, the SC, the PBG and the Pn in the
224 brain are labeled by GFP. Scale bar: 10 μm. (**C**) Experimental strategy for ablating the SC-
225 projected GABAergic RGCs (phase 1: Expressing FLP in the EYFP-labeled GABAergic
226 RGCs; phase 2: DTA expression via the FLP/FDIO system; phase 3: DTA-induced
227 apoptosis). The SC-projected GABAergic RGCs can be effectively eliminated. (**D-G**) With
228 the expanding looming stimulus at 2-20 degrees for 0.6 second, representative movement
229 traces of the control (VEH) and DTA-expressed (DTA+FLP) *vGAT-Cre* (top, **E**) and *Gad2-*
230 *Cre* (bottom, **E**) mice. **F** and **G**: quantification results on the movement distance and the time

interval from the start to the end point, respectively. (**H**-**J**) c-Fos positive cells in SC and PBG in looming stimulated control mice (**H**) and DTA+FLP treated mice (**I**). **J**: quantification results on c-Fos positive cells in SC (top) and PBG (bottom) in each group of mice. Mann-Whitney U test; **: $P<0.01$, ***: $P<0.001$, ****: $P<0.0001$. Scale bar: 50 μm.

spgRGCs are dispensable for image forming functions and the pupillary light reflex (PLR)

Electroretinography (ERG) and the optomotor response were used to investigate if spgRGCs are required for image-forming functions. There were no significant changes in the a-wave and b-wave amplitudes of scotopic ERGs between the control and ablation groups, indicating that spgRGCs are dispensable for overall retinal functions (Fig. 5A-B). The optomotor response was used to determine visual acuity based on head movements in response to the moving vertical grating stimulus. There was no significant difference in the visual acuity between the control and ablation groups (Fig. 5C-G). The PLR is characterized by a light-induced rapid pupil constriction followed by rapid partial re-dilation at light offset[50]. Similarly, there was no significant difference in light-triggered pupillary constriction between the control and ablation groups (Fig. 5H and 5I). Therefore, these results indicate that spgRGCs are not required for visual image formation and PLR.

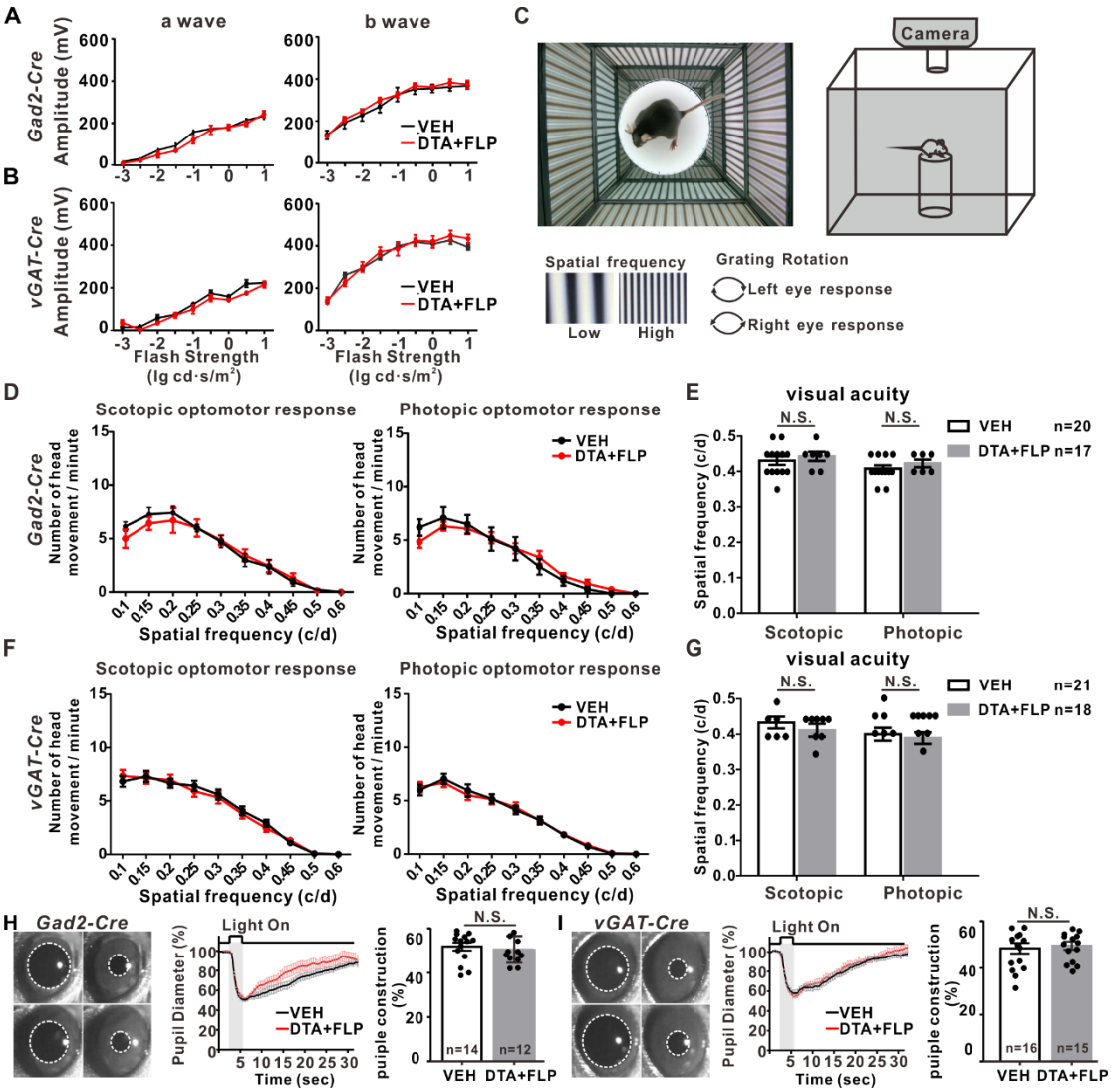

Figure 5. spgRGCs are dispensable for innate visual functions. (**A, B**) ERG amplitudes of a-wave (left) and b-wave (right) show no significant changes in the ablation groups. (**C-G**) A grating stimulation-based OMR setup (**C**), there are no significant differences on the optomotor response (**D**, **F**) and the maximum spatial frequency (visual acuity; **E**, **G**) under scotopic and photopic conditions in the control or DTA+FLP induced ablation groups. (**H**, **I**) There are no significant changes on the pupil diameters of *Gad2-Cre* (**H**) and *vGAT-Cre* (**I**) mice in response to chromatic light stimulation (blue light: 300 lux, 3 s) following the ablation of spgRGCs. Left: infrared images; middle: traces of pupil diameter changes

following light stimulation; Right: pupil constriction (% of the pupil diameters before light simulation).

GABA released from the spgRGCs govern the looming-evoked flight response

Aiming at removing the effect of ablating spgRGCs on the structural integrity of neural circuits, adeno-associated virus (AAV) with short hairpin (shRNA) against vGAT was adopted to knock down vGAT expression by injecting rAAV-U6-Loxp-CMV-EGFP-SV40-polyA-Loxp-shRNA(vGAT shRNA group) into the vitreous of the *vGAT-Cre* mice (Fig. 6A). In order to assess the effectiveness and tissue-specificity of the *vGAT-Cre* combining with LoxP-shRNA system, western blot analysis indicated that the system was in position to efficiently silence vGAT in retina. Retina transfected with vGAT shRNA in two months manifested an inferior expression of vGAT protein to the Control (scramble shRNA group) (Fig. 6B). Afterwards, the looming behavior produced by knockdown vGAT in the spgRGCs was compared, vGAT shRNA group conveyed an increased escape latencies and duration during the trials in contrast with the Control group (Fig. 6C-D, Supplemental Movie 5-6). In addition, there was no significant diversity between the Control shRNA and the vGAT shRNA group in the optomotor response (Fig. S3). In a word, findings mentioned above demonstrate that functional release of GABA from spgRGCs are required for the looming-evoked flight response (L. Huang et al., 2017).

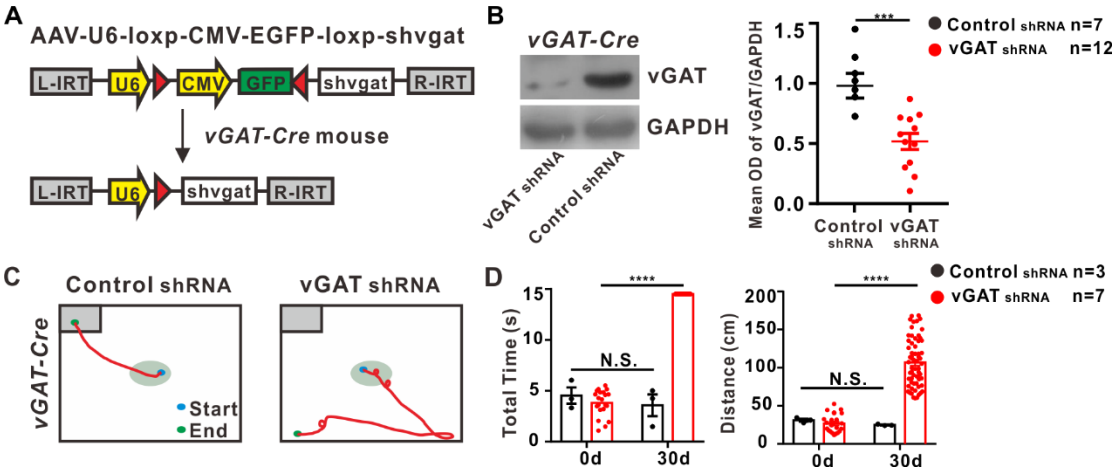

Figure 6. Looming-evoked flight response requires functional release of GABA from spgRGCs. (**A**) The hairpin (sh) oligonucleotide (sholigo), targeting the vGAT transcript, was used to knock down vGAT expression. (**B**) Western blot analysis show that it can efficiently knockdown vGAT. Representative immunoreactive bands of vGAT protein levels, the bottom panel show the mean optical density (OD) of the band corresponding to vGAT normalized to GAPDH in the two groups. (**C-D**) Typical movement traces of the Control shRNA and vGAT shRNA groups. (**D**) Before or 30 days after injection. Quantification results on the movement distance and the time interval from the start to the end point, respectively. Mann-Whitney U test; ***: $P<0.001$, ****: $P<0.0001$.

Discussion

The ability to detect rapidly approaching objects, which mimic predators, is a highly conserved innate defensive behavior in *Drosophila*, naïve rodents (Blanchard, Mast, & Blanchard, 1975) and primates (Wiener & Levine, 1992). Although the looming-evoked neural circuits in the mouse brain have been nicely studied, it remains poorly understood how the visual looming stimulus is transmitted from the retina to the brain. Here, we show that mouse spgRGCs directly innervate PV^+ SC neurons to mediate the looming-evoked flight behavior through the SC-PBGN pathway. In the adult mouse retina, GABAergic RGCs project their axons to multiple brain areas, including SC, SCN, OPN and LGN. Moreover, approximately 13% RGCs are GABAergic and belong to ON, OFF and ON-OFF RGC subtypes. In addition, the SC-projected GABAergic RGCs can release the inhibitory GABA to their mono-synapsed SC neurons when activated. Finally, DTA-mediated ablation of those spgRGCs causes the loss of the looming-evoked flight response. Therefore, we identify a novel GABAergic RGC population in the mouse retina that projects and releases GABA to the SC, and have further demonstrated that spgRGCs function as a part of the neural circuitry mediating the looming-evoked defensive behavior.

In the mammalian eye, RGCs are the only cell type sending long axons to connect the retina to the brain. Earlier studies suggest the existence of GABA-like immunoreactive RGCs in turtle (Hurd & Eldred, 1989) , bufo (Gabriel, Straznicky, & Wye-Dvorak, 1992) and rabbit

retinas (Yu et al., 1988). Since GABAergic neurons are believed to function within short distances to regulate local neural networks (Harris & Shepherd, 2015; Z. J. Huang, 2014; Kepecs & Fishell, 2014), the existence of GABAergic RGCs have not been taken seriously. In this study, we have provided three pieces of experimental evidence to demonstrate the existence of GABAergic RGCs in the adult mouse retina. First, *Gad2-Cre* and *vGAT-Cre*-driven Cre-dependent expression of EYFP reliably label RGCs that project axons to the brain. *Gad2* and *vGAT* (also known as *Slc32a1*) encode a GABA synthesizing enzyme and a vesicular GABA transporter, respectively, which are both known to be expressed in GABAergic neurons (Chan et al., 2017; Garcia-Junco-Clemente et al., 2017; Latremoliere et al., 2018). Consistently, those EYFP-labeled RGCs also express GABA. Second, by re-analyzing the recently published RGC SC-seq results (Kakizaki, Oriuchi, & Yanagawa, 2015), we have found that 13% of RGCs express *Gad2*. Interestingly, most of the 40 RGC subgroups identified by SC-seq, including melanopsin-positive intrinsically photosensitive RGCs (ipRGCs), also express *Gad2* mRNA. Third, optogenetic activation drives EFYP-labeled RGCs to release GABA and elicit the IPSC responses in the projected SC neurons, indicating that those EYFP-labeled RGCs are bona fide GABAergic neurons. Finally, our AAV-mediated tracing experiments have shown that those EYFP-labeled GABAergic RGCs project their axons to the four major brain regions, SCN, OPN, LGN and SC. The SCN and OPN brain areas are required for non-image-forming functions, circadian photoentrainment (Brown et al., 2010; Ecker et al., 2010; Hattar et al., 2006), and the pupillary light reflex (PLR) (Bonmati-Carrion et al., 2016), respectively. The LGN is required for visual image-

323 forming functions, whereas the SC is required for both non-image-forming and image-
324 forming functions (Marcelja, 1979; Sylvester, Haynes, & Rees, 2005). Taken together,
325 multiple types of GABAergic RGCs exist in the adult mouse retina and likely have distinct
326 biological functions.

327 This study functionally demonstrates that spgRGCs participate in the looming-evoked
328 innate flight response via the SC-PBGN pathway. Based on stratification within the IPL and
329 light-mediated responses, spgRGCs are composed of ON, OFF and ON-OFF types. Those
330 spgRGCs primarily target the superficial and intermediate layers of the SC, which are known
331 to be required for the looming-evoked defensive behavior (Ito & Feldheim, 2018; Liang et al.,
332 2015). Indeed, DTA-mediated ablation of spgRGCs diminishes the looming-evoked flight
333 response, but does not affect image-forming and other non-image-forming functions. Dual
334 SC/DRN-projected RGCs have been previously identified for the looming-evoked flight
335 response (L. Huang et al., 2019). Since newly identified spgRGCs do not project to the DRN,
336 SC/DRN-projected RGCs and spgRGCs represent two distinct RGC populations for
337 mediating the looming-evoked flight response. Our trans-synaptic tracing results indicate that
338 the GABAergic RGC-projecting SC neurons are also PV^+ and are capable of innervating
339 PBGN, PN and DLG in the brain, which should be the same as the previously identified PV^+
340 glutamatergic SC neurons (Shang et al., 2015). Those PV^+ SC neurons activate the PBGN-
341 amygdala circuitry to control the looming-evoked flight response (Shang et al., 2019; Shang
342 et al., 2015). Our c-Fos expression results also support that spgRGCs activate PV^+ SC and

PGBN neurons to mediate the looming-evoked flight response. Therefore, this study shows that spgRGCs are mono-synaptically connected to the SC-PBGN circuitry for mediating the looming-evoked flight behavior through GABA. This study has also opened the door for studying other biological functions of GABAergic RGCs.

Materials and Methods

Animals

The mouse strains used: C57BL/6, *vGAT-Cre* [*B6J.129S6(FVB)-Slc32a1*$^{tm2(cre)Lowl}$*/ MwarJ*; Jackson Laboratory] and *Gad2-Cre* (*B6J.Cg-Gad2*$^{tm2(cre)Zjh}$*/MwarJ*; Jackson Laboratory). All mice were group-housed and maintained on a 12h light/12h dark cycle with food and water provided *ad libitum*. 6-8-week old adult males were randomly divided into experimental and control groups. All the experiments were done in accordance with the guidelines of Wuhan University Institutional Animal Care Committee.

Stereotaxic injection of AAV and HSV

For cell-type-specific retrograde tracing, animals were first anesthetized by intraperitoneally injecting ketamine and xylazine (60 and 16 mg/kg body weight, respectively). Following the making of a small craniotomy hole by a dental drill (OmniDrill35, WPI), a micropipette controlled by a Quintessential Stereotaxic Injector system (Stoelting, Wood Dale, IL, USA, Micro4; WPI, Sarasota, USA) was used to inject 700 nl *AAV2/retro-EF1a-DIO-EYFP-EYFP-*

WPRE-pA (6.48×10^{12} vg/ml, BrainVTA, Wuhan) virus into the SC of control, *Gad2-Cre* and *vGAT-Cre* mice. Coordinates targeting the SC were as follows: 3.9 mm back from the bregma (anteroposterior), 0.45 mm lateral to the midline (mediolateral), and 1.7 mm deep (dorsoventral) below the pial surface. The pipette was held in place for 10 min, and then withdrawn slowly (Gauvain & Murphy, 2015).

For anterograde RGCs tracing, a small incision was made in the conjunctiva to expose the sclera, and 1.5 μl of *AAV2/2-EF1a-DIO-EYFP-EYFP-WPRE-pA* (2.12×10^{12} vg/ml, BrainVTA, Wuhan) suspension was injected into the center of the vitreous cavity through the ora serrata with a Hamilton syringe (Hamilton Company, Reno, NV). For anterograde trans-synaptic tracing, 1.5 μl of *HSV-LSL-TK-G4* (1×10^{10} vg/ml) suspension was injected into the vitreous chamber, and brain slice were obtained at 6 days (Lo & Anderson, 2011). For ablating SC-projecting GABAergic RGCs, two viruses were performed sequentially. 700 nl of *AAV2/retro-EF1a-DIO-FLP-WPRE-pA* (7.33×10^{12} vg/ml, BrainVTA, Wuhan) was first injected into the SC of *vGAT-Cre/Gad2-Cre* mice, and 1.5 μl of *AAV2/2-EF1α-FDIO-DTA-WPRE-pA* (6.2×10^{12} vg/ml, BrainVTA, Wuhan) or PBS (as a control) was then injected into the vitreous chamber bilaterally 3 days later. GABAergic RGC degeneration were detected after one month (Gauvain & Murphy, 2015; Hu et al., 2017). All the experiments with viruses were performed in bio-safety level 2 (BSL-2) laboratory and animal facilities.

379 To remove the putative GABAergic regulation on looming-evoked flight response from
380 spgRGCs, we used vGAT-selective hort hairpin (shRNA) constructs to knock down vGAT
381 expression in the retina by injecting vectors into the vitreous of the *vGAT-Cre* mice. The
382 modified U6 promoter harbors a LoxP-CMV-EGFP-LoxP inside. When the vGAT positive cell
383 was coinfected with LoxP-shRNA vectors, Cre-mediated recombination results in subsequently
384 cuts the LoxP-CMV-eGFP-LoxP inside the U6 promoter and activates the U6 promoter. The
385 activated U6 promoter then drives the down-stream shRNA expression and silences the target
386 gene. rAAV-U6-Loxp-CMV-EGFP-SV40-polyA-Loxp-shRNA(shvgat) and rAAV-U6-Loxp-
387 CMV-EGFP-Loxp-shRNA(scramble/Control) were injected into the vitreous chamber. AAVs
388 carrying an shRNA outside two loxP sites (AAV-U6-LoxP-CMV-GFP-LoxP-shRNA, 6.3×10^{12}
389 vg/ml) (BrainVTA, Wuhan) were used for Cre-dependent silencing of vGAT in the *vGAT-Cre*
390 mice. The shRNA oligonucleotides for targeting vGAT mRNA (shvgat; 5′-TGCTGTTG
391 ACAGTGAGCGCGGTGTGCTCGTGGTGAATAAGTAGTGAAGCCACAGATGTACTTAT
392 TCACCACGAGCACACCATGCCTACTGCCTCGGA-3′) and control shRNA (Control; 5′
393 -TGCTGTTGACAGTGAGCGGCCGCGATTAGGCTGTTATAATAGTGAAGCCACAGAT
394 GTATTATAACAGCCTAATCGCGGCTGCCTACTGCCTCGGA-3′) were created following
395 the information described in the literature (Gangadharan et al., 2016; Peng et al., 2013;
396 Stegmeier, Hu, Rickles, Hannon, & Elledge, 2005). Control shRNA sequences were used to
397 construct a non-targeting control virus. Mice were given injections of either vGAT shRNA or
398 non-targeting scramble shRNA (Control shRNA).

399 **Histological procedures**

400 For retina whole mounts, eyes were enucleated after cervical dislocation, and eye cups were
401 fixed in 4% paraformaldehyde (PFA; pH 7.4) at room temperature for 40 min (Jain et al.,
402 2016). Retina was isolated from the eye cup and flattened. For retina cryosections, eyecups
403 were fixed in 4% paraformaldehyde for 40 min, washed with PBS three times for 5 minutes,
404 incubated sequentially for 1 h in 10% and 20% sucrose, overnight in 30% sucrose. Then the
405 eyes were embedded in O.C.T compound (Sakura Finetek, Japan) and frozen at -80°C.
406 Retinal sections were cut at 14 μm thickness on a freezing microtome (Leica, CM1950,
407 Germany) and mounted on gelatin-coated slides (Chen, Luo, Liu, & Shen, 2018). For brain
408 cryosections, after transcranial perfusion with 0.9% saline followed by 4% paraformaldehyde
409 in 0.1 M of PBS, the brain was removed and post-fixed with 4% paraformaldehyde for 1 day
410 at 4 ℃, then transferred into a 30% sucrose solution for 3 days until sectioning with a
411 cryostat. A series of 50 μm sections were collected for staining.

412 **Immunostaining**

413 The procedures of immunohistochemistry refer to the previous work (Kircher, Crippa, Martin,
414 Kawasaki, & Kostic, 2019) (the retina and brain slices were first incubated for 2 hours in a
415 blocking solution containing 5% bovine serum albumin (BSA), and 0.2% Triton X-100 in
416 PBS (pH 7.4). And then incubated in primary antibodies at 4°C overnight. After washing with
417 PBS for 3x15 min, the samples were incubated in the appropriate secondary antibodies for 2
418 hours at room temperature. The samples were washed again in PBS for 3x15 min and

mounted in DAPI (4-,6-diamidino-2-phenylindole; Life Technologies, D1306) for 5 min. The antibodies used in this work were list as follows: chicken polyclonal antibody against GFP for immunolabeling EYFP+/GFP+ neurons (1:2000, Abcam, ab13970); mouse polyclonal antibody against Brn3a (1:500, Millipore, MAB1585); goat polyclonal antibody against ChAT (1:200, Millipore, AB144P); rabbit polyclonal antibody against GABA (1:200, Sigma, A2052), rabbit polyclonal antibody against c-Fos (1:500; PC38T, Calbiochem). Secondary antibodies were anti-isotypic Alexa Fluor conjugates (1:1000, Invitrogen), incubation for 2 h at room temperature, and after washes in PBS, the retinas were subsequently mounted in antifade mounting medium.

Confocal microscopy and three-dimensional reconstruction

Images were collected with a confocal laser-scanning microscope (Leica, SP8). For three-dimensional reconstruction of injected or virus labelled RGCs, the Z-axis interval was set at 0.4 μm and areas of interest were scanned with a 100X oil immersion objective. A montage of optical section stacks was created, projected to a 0° X-Y plane and a 90° X-Z plane to obtain a 3-D reconstruction. Each stack of optical sections covered a retinal area of 325.75 x 325.75 μm^2 (1,024x1,024 pixels). Details of three-dimensional reconstruction and confocal calibration procedures were described elsewhere (Ren et al., 2013). Contrast and brightness were adjusted. Total soma and dendritic field size of each filled cell were analyzed.

Electrophysiological recording on tissue slices

Brain slices containing the SC were prepared recording to the procedures described previously (L. Huang et al., 2019). In brief, mice were anesthetized with isoflurane. After decapitation, brains were immediately immersed in ice-cold oxygenated (95% O_2 and 5% CO_2) cutting solution which containing (in mM): Choline chloride 97, Ascorbic acid 11, KCl 2.5, $NaHCO_3$ 25, NaH_2PO_4 1.26, Sodium Pyruvate 3, $CaCl_2$ 0.5, $MgCl_2$ 7.2, glucose 25. Brain slices (350 μm) was cut using a vibratome (VT1200S, Leica, Germany). The slices were incubated in 34ºC artificial cerebrospinal fluid (ACSF: NaCl 118, KCl 2.5, $CaCl_2$ 2, NaH_2PO_4 1, $MgCl_2$ 2, $NaHCO_3$ 26 and glucose 22 in mM) and bubbled with 95% O_2 and 5% CO_2 for 30 minutes before transfer to the recoding chamber. After an hour incubation at room temperature (25ºC), slice was transferred to the recording chamber, visualized with an X40 water immersion lens, DIC optics (BX51WI, Olympus, Japan) and a CCD camera (IR1000, DAGE-MTI, USA). The data were digitized and recorded on-line using Clampex 10.6 (Axon Instruments, Molecular Devices). Signals were amplified by MultiClamp 700B (Molecular Devices), filtered at 1 kHz and sampled at 10 kHz. Electrodes were fabricated from borosilicate glass (Sutter instrument) using a pipette puller (Sutter, P1000); with resistance 5-7 MΩ. The internal solution for the recording glass pipette was (in mM): Cs-methanesulfonate 115, CsCl 20, HEPES 10, $MgCl_2$ 2, ATP-Mg 4, GTP-Na 0.4, Na-phosphocreatine 10, EGTA 0.6 (pH 7.2 adjusted by CsOH, mOsm 290). After establishing the whole-cell configuration, the holding potential was maintained at 0 mV and GABA receptor-mediated IPSCs were pharmacologically isolated using an antagonist cocktail (D-AP5 50 μM; strychnine 10 μM, CNQX 10 μM and

458 TTX 1 μM)(Yang & Ma, 2011). ChR2-induced synaptic current was recorded while holding at
459 -70 mV. The external solution contained NaCl 125, KCl 2.5, $CaCl_2$ 2, $MgSO_4$ 1, $NaHCO_3$ 26,
460 NaH_2PO_4 1.25 and Glucose 20. All drugs were obtained from Sigma-Aldrich or Tocris
461 Bioscience.

462 For light stimulation, an optic fiber was positioned right above the slice (Mightex, BioLED
463 Light). Synchronized light-evoked response was triggered by Clampex 10 to deliver light
464 pulses (470 nm, 5 ms, 0.05 Hz). For retinal slice recording, the isolated retinas were cut into
465 15-μm-thick slices in Ringer's using a manual cutter (ST-20, Narishige, Japan). The slices
466 were transferred into a recording chamber with the cut side up and held in place with vaseline.
467 Whole-cell recordings were obtained from selected neurons. ChR2 positive GABAergic
468 neurons was confirmed by enhanced yellow fluorescent protein (eYFP) labeling.

469 **Looming stimulation test**

470 The looming stimulation test was performed in an open-top acrylic box, as described by
471 Huang L, et al (L. Huang et al., 2017) . The arena had dim lighting from the screen of the
472 monitor. The floor and three walls were covered with a frosted coating to prevent reflections
473 of the stimulus. A camera from the side was used to track the movements. An LED monitor
474 was embedded in the ceiling to present the looming stimulus. The stimulus program was
475 displayed on a LED monitor (HPZ24i). The looming stimulus, which consisted of an
476 expanding black disc, appeared at a diameter of a visual angle from 2° to 20° in 0.6 s, for 15

477 times in 14.6 s. The stimulation was initiated manually when the mouse was in the center of
478 the arena (Hu et al., 2017; L. Huang et al., 2017; Yilmaz & Meister, 2013). Looming tests
479 were conducted in Control mice (n=22 for *Gad2-Cre* mice; 28 for *vGAT-Cre* mice) and
480 DTA+FLP mice (n=43 for *Gad2-Cre* mice; 35 for *vGAT-Cre* mice).

481 **Optomotor response**

482 Optomotor responses of animals in Control (n=20 for *Gad2-Cre* mice; n=21 for *vGAT-Cre*
483 mice) and DTA+FLP (n=17 for *GAD-Cre* mice; n=18 for *vGAT-Cre* mice) groups were
484 measured as described (Abdeljalil et al., 2005). Briefly, mice were placed on a platform (9 cm
485 diameter, 17.5 cm above the bottom of the mirror) surrounded by four LCD screens (Lenovo,
486 L1900 PA) that displayed rotating black-and-white stripes at various spatial frequencies. The
487 platform was set in the middle of the arena for mouse to stand and move freely. Stimuli were
488 presented on four computer screens surrounding the animal covering the whole field of view
489 with a texture projected onto the surface of a virtual sphere. Mice were videotaped with a
490 camera mounted on top of the platform for subsequent scoring of head tracking movements.
491 Animals were dark-adapted for 3-4 hours, and then presented with vertical black and white
492 stripes of a defined spatial frequency. These stripes were rotated alternately clockwise and
493 anticlockwise for 30 s in each direction and paused for 10 s. The animals were tested with
494 spatial frequencies increasing from 0.1 to 0.6 cycles per degree (cyc/deg): 0.1, 0.15, 0.2, 0.25,
495 0.3, 0.35, 0.4, 0.45, 0.5 and 0.6 cyc/deg. Procedures for measuring optomotor responses under

496 photopic condition were similar to the scotopic condition except that animals were subjected
497 to 400 Lux light stimulus for 10 mins to allow them to adapt to the light.

498 **Pupillary light reflex**

499 Mice were dark-adapted overnight and tested in a dark room. Mice were unanesthetized and
500 restrained by hand. We handled the mice for several days prior to the experiments to get them
501 accustomed to the tester and make sure the animal calming during the experiments as stress
502 might affect the pupil size (Kostic et al., 2016). Any mice that showed signs of stress,
503 including vocalizations and wriggling during the experiments, we will suspend the recording
504 and comfort the animal until they are calm again. The light stimulus was conducted by a LED
505 light (470 nm, 3s, Mightex BioLED Light). The changes of pupil size were monitored by an
506 infrared camera (IR1000, DAGE-MTI, USA). The recording started 2.5 s before the light
507 stimulus and continued for 30 s after the stimulus. The images were made grayscale and then
508 brightness and contrast were adjusted to enhance visibility of the pupil and exported. Pupil
509 diameters were converted to a percentage of the baseline. The averaged response from pupil
510 recordings (Control: n=14 for *Gad2-Cre*, n=16 for *vGAT-Cre* mice; DTA+FLP: n=12 for
511 *Gad2-Cre*, n=15 for *vGAT-Cre* mice) was calculated and plotted through GraphPad Prism 6
512 software (GraphPad Software, Inc., San Diego, CA, USA).

513 **Electroretinography**

514 Retinal functions of control (n=16 for *Gad2-Cre* and *vGAT-Cre*) and DTA+FLP (n=24 for
515 *Gad2-Cre* and *vGAT-Cre*) mice were measured with a commercial ERG system (RetiMINER,
516 China). After overnight dark adaptation(Mees et al., 2019), the mice were anesthetized by
517 intraperitoneally injecting ketamine and xylazine (60 mg/kg and 16 mg/kg bodyweight,
518 respectively), and then lightly secured to a stage with fastener strips across the back to ensure
519 a stable, reproducible position for ERG recordings. All procedures were performed under dim
520 red light. Customized gold-loop wire electrodes were placed on the center of each eye to
521 measure the electrical response of the eye to flash stimulation. Reference electrodes were
522 placed subcutaneously between the ears and a ground electrode was placed in the base of the
523 tail. The ERG consisted of a 9-step series of full-field flash stimuli dark-adapted (-3 to 1 lg
524 cd·s/m^2) conditions. After the ERG recording, erythromycin was used on the ocular surface,
525 and the animals were allowed to recover on a heating pad (Su et al., 2016).

526 **Western blotting**

527 Western blotting was performed according to previous work on retinal extracts (Chen et al.,
528 2018). They were homogenized with RIPA lysis buffer (Thermo Scientific, USA) supplemented
529 with a PMSF (Servicebio, Wuhan). Protein concentration in the supernatant was measured
530 using BCA Protein Assay kit (Servicebio, Wuhan). Proteins (40 μg) in retinal samples were
531 resolved by 10% sodium dodecyl sulphate polyacrylamide gel electrophoresis (SDS-PAGE)
532 and transferred onto and electro-blotted to nitro-cellulose membranes (Millipore, USA). The

membranes were subsequently blocked with 5% nonfat milk for one hour and incubated overnight at 4 °C with primary antibodies, including rabbit anti-SLC32A1 (1:1000; Absin, abs136723), rabbit anti-GAPDH (1:6000; Antgene, ANT012). The membranes were washed for 30 min in TBS-Tween 20 and incubated with HRP-conjugated goat anti-rabbit IgG (1:5000, Servicebio) for 2 h at RT. After the second antibody, the membranes were washed again and immunoreactive bands were subsequently detected using ECL reagents and recorded by X-ray films.

Data quantification and statistical Analysis

All experiments were performed with anonymized samples in which the experimenter was unaware of the experimental condition of mice. Statistical analysis was performed using SPSS software (IBM, Armonk, NY, USA). Unpaired *t-test* or Mann-Whitney U test were used. Error bars represent the mean ± standard error of mean (SEM). $p<0.05$ is considered as significant difference between two samples (Chen et al., 2018; Dinculescu et al., 2016).

Author Contributions

Conception and design of the experiments: Y. Shen and X. Luo. Performed the experiments: X. Luo, Q. Deng, D. Cai and K. Shen. Analysis and interpretation of data: Y. Shen, T. Xie, X. Luo, D. Cai, K. Shen and H. Li. Wrote the paper: T. Xie, Y. Shen, and X. Luo. All authors approved the final version for publication.

Acknowledgments

This work was supported by grants from the National Key R&D Program of China (2017YFE013400 to Y.S.), the National Nature Science Foundation of China (81470628 Y. S. 81800872 to Q.D.) and The Stowers SIMR fund (to T. X.).

Conflict of interest

The authors of this work do not have any conflicts of interest.

References

Abdeljalil J., Hamid M., Abdel-Mouttalib O., Stephane R., Raymond R., Johan A., Jose S., Pierre C., & Serge P. (2005). The optomotor response: a robust first-line visual screening method for mice. *Vision Res., 45*(11), 1439-1446. doi:10.1016/j.visres.2004.12.015

Baden T., Berens P., Franke K., Roman Roson M., Bethge M., & Euler T. (2016). The functional diversity of retinal ganglion cells in the mouse. *Nature, 529*(7586), 345-350. doi:10.1038/nature16468

Ball W., & Tronick E. (1971). Infant responses to impending collision: optical and real. *Science, 171*(3973), 818-820. doi:10.1126/science.171.3973.818

Blanchard R. J., Mast M., & Blanchard D. C. (1975). Stimulus control of defensive reactions in the albino rat. *J Comp Physiol Psychol, 88*(1), 81-88. doi:10.1037/h0076213

Bonmati-Carrion M. A., Hild K., Isherwood C., Sweeney S. J., Revell V. L., Skene D. J., Rol M. A., & Madrid J. A. (2016). Relationship between Human Pupillary Light Reflex and Circadian System Status. *PLoS One, 11*(9), e0162476. doi:10.1371/journal.pone.0162476

Brown T. M., Gias C., Hatori M., Keding S. R., Semo M., Coffey P. J., Gigg J., Piggins H. D., Panda S., & Lucas R. J. (2010). Melanopsin contributions to irradiance coding in the thalamo-cortical visual system. *PLoS Biol., 8*(12), e1000558. doi:10.1371/journal.pbio.1000558

Chan K. Y., Jang M. J., Yoo B. B., Greenbaum A., Ravi N., Wu W. L., Sanchez-Guardado L., Lois C., Mazmanian S. K., Deverman B. E., & Gradinaru V. (2017). Engineered AAVs for efficient noninvasive gene delivery to the central and peripheral nervous systems. *Nat. Neurosci., 20*(8), 1172-1179. doi:10.1038/nn.4593

Chen Y., Luo X., Liu S., & Shen Y. (2018). Neuroprotective effect of cannabinoid receptor 1 antagonist in the MNU-induced retinal degeneration model. *Exp. Eye Res., 167*, 145-151. doi:10.1016/j.exer.2017.11.001

Chou X. L., Wang X., Zhang Z. G., Shen L., Zingg B., Huang J., Zhong W., Mesik L., Zhang L. I., & Tao H. W. (2018). Inhibitory gain modulation of defense behaviors by zona incerta. *Nat Commun, 9*(1), 1151. doi:10.1038/s41467-018-03581-6

Collier R. J. (2001). Understanding the mode of action of diphtheria toxin: a perspective on progress during the 20th century. *Toxicon, 39*(11), 1793-1803. doi:10.1016/s0041-0101(01)00165-9

Dinculescu A., Stupay R. M., Deng W. T., Dyka F. M., Min S. H., Boye S. L., Chiodo V. A., Abrahan C. E., Zhu P., Li Q., Strettoi E., Novelli E., Nagel-Wolfrum K., Wolfrum U., Smith W. C., & Hauswirth W. W. (2016). AAV-Mediated Clarin-1 Expression in the Mouse Retina: Implications for USH3A Gene Therapy. *PLoS One, 11*(2), e0148874. doi:10.1371/journal.pone.0148874

Ecker J. L., Dumitrescu O. N., Wong K. Y., Alam N. M., Chen S. K., LeGates T., Renna J. M., Prusky G. T., Berson D. M., & Hattar S. (2010). Melanopsin-expressing retinal ganglion-cell photoreceptors: cellular diversity and role in pattern vision. *Neuron, 67*(1), 49-60. doi:10.1016/j.neuron.2010.05.023

Fang Y. Y., Yamaguchi T., Song S. C., Tritsch N. X., & Lin D. (2018). A Hypothalamic Midbrain Pathway Essential for Driving Maternal Behaviors. *Neuron, 98*(1), 192-207 e110. doi:10.1016/j.neuron.2018.02.019

Gabriel R., Straznicky C., & Wye-Dvorak J. (1992). GABA-like immunoreactive neurons in the retina of Bufo marinus: evidence for the presence of GABA-containing ganglion cells. *Brain Res., 571*(1), 175-179. doi:10.1016/0006-8993(92)90528-h

Gangadharan G., Shin J., Kim S.-W., Kim A., Paydar A., Kim D.-S., Miyazaki T., Watanabe M., Yanagawa Y., Kim J., Kim Y.-S., Kim D., & Shin H.-S. (2016). Medial septal GABAergic projection neurons promote object exploration behavior and type 2 theta rhythm. *Proc. Natl. Acad. Sci. U.S.A., 113*(23), 6550-6555. doi:10.1073/pnas.1605019113

Garcia-Junco-Clemente P., Ikrar T., Tring E., Xu X., Ringach D. L., & Trachtenberg J. T. (2017). An inhibitory pull-push circuit in frontal cortex. *Nat. Neurosci., 20*(3), 389-392. doi:10.1038/nn.4483

Gauvain G., & Murphy G. J. (2015). Projection-specific characteristics of retinal input to the brain. *J. Neurosci., 35*(16), 6575-6583. doi:10.1523/JNEUROSCI.4298-14.2015

Gibson W. T., Gonzalez C. R., Fernandez C., Ramasamy L., Tabachnik T., Du R. R., Felsen P. D., Maire M. R., Perona P., & Anderson D. J. (2015). Behavioral responses to a repetitive visual threat stimulus express a persistent state of defensive arousal in Drosophila. *Curr Biol, 25*(11), 1401-1415. doi:10.1016/j.cub.2015.03.058

Harris K. D., & Shepherd G. M. (2015). The neocortical circuit: themes and variations. *Nat. Neurosci., 18*(2), 170-181. doi:10.1038/nn.3917

Hattar S., Kumar M., Park A., Tong P., Tung J., Yau K. W., & Berson D. M. (2006). Central projections of melanopsin-expressing retinal ganglion cells in the mouse. *J. Comp. Neurol., 497*(3), 326-349. doi:10.1002/cne.20970

Hirano A. A., Brandstatter J. H., & Brecha N. C. (2005). Cellular distribution and subcellular localization of molecular components of vesicular transmitter release in horizontal cells of rabbit retina. *J Comp Neurol, 488*(1), 70-81. doi:10.1002/cne.20577

Hu Y., Chen Z., Huang L., Xi Y., Li B., Wang H., Yan J., Lee T. M. C., Tao Q., So K. F., & Ren C. (2017). A translational study on looming-evoked defensive response and the underlying subcortical pathway in autism. *Sci Rep, 7*(1), 14755. doi:10.1038/s41598-017-15349-x

Huang L., Xi Y., Peng Y., Yang Y., Huang X., Fu Y., Tao Q., Xiao J., Yuan T., An K., Zhao H., Pu M., Xu F., Xue T., Luo M., So K. F., & Ren C. (2019). A Visual Circuit Related to Habenula Underlies the

Antidepressive Effects of Light Therapy. *Neuron, 102*(1), 128-142 e128. doi:10.1016/j.neuron.2019.01.037

Huang L., Yuan T., Tan M., Xi Y., Hu Y., Tao Q., Zhao Z., Zheng J., Han Y., Xu F., Luo M., Sollars P. J., Pu M., Pickard G. E., So K. F., & Ren C. (2017). A retinoraphe projection regulates serotonergic activity and looming-evoked defensive behaviour. *Nat Commun, 8*, 14908. doi:10.1038/ncomms14908

Huang Z. J. (2014). Toward a genetic dissection of cortical circuits in the mouse. *Neuron, 83*(6), 1284-1302. doi:10.1016/j.neuron.2014.08.041

Hurd L. B., & Eldred W. D. (1989). Localization of GABA- and GAD-like immunoreactivity in the turtle retina. *Vis. Neurosci., 3*(1), 9-20. doi:10.1017/s0952523800012463

Ito S., & Feldheim D. A. (2018). The Mouse Superior Colliculus: An Emerging Model for Studying Circuit Formation and Function. *Front Neural Circuits, 12*, 10. doi:10.3389/fncir.2018.00010

Jain V., Srivastava I., Palchaudhuri S., Goel M., Sinha-Mahapatra S. K., & Dhingra N. K. (2016). Classical Photoreceptors Are Primarily Responsible for the Pupillary Light Reflex in Mouse. *PLoS One, 11*(6), e0157226. doi:10.1371/journal.pone.0157226

Kakizaki T., Oriuchi N., & Yanagawa Y. (2015). GAD65/GAD67 double knockout mice exhibit intermediate severity in both cleft palate and omphalocele compared with GAD67 knockout and VGAT knockout mice. *Neuroscience, 288*, 86-93. doi:10.1016/j.neuroscience.2014.12.030

Kepecs A., & Fishell G. (2014). Interneuron cell types are fit to function. *Nature, 505*(7483), 318-326. doi:10.1038/nature12983

Kircher N., Crippa S. V., Martin C., Kawasaki A., & Kostic C. (2019). Maturation of the Pupil Light Reflex Occurs Until Adulthood in Mice. *Front. Neurol., 10*, 56. doi:10.3389/fneur.2019.00056

Kostic C., Crippa S. V., Martin C., Kardon R. H., Biel M., Arsenijevic Y., & Kawasaki A. (2016). Determination of Rod and Cone Influence to the Early and Late Dynamic of the Pupillary Light Response. *Invest Ophthalmol Vis Sci, 57*(6), 2501-2508. doi:10.1167/iovs.16-19150

Latremoliere A., Cheng L., DeLisle M., Wu C., Chew S., Hutchinson E. B., Sheridan A., Alexandre C., Latremoliere F., Sheu S. H., Golidy S., Omura T., Huebner E. A., Fan Y., Whitman M. C., Nguyen E., Hermawan C., Pierpaoli C., Tischfield M. A., Woolf C. J., et al. (2018). Neuronal-Specific TUBB3 Is Not Required for Normal Neuronal Function but Is Essential for Timely Axon Regeneration. *Cell Rep, 24*(7), 1865-1879 e1869. doi:10.1016/j.celrep.2018.07.029

Liang F., Xiong X. R., Zingg B., Ji X. Y., Zhang L. I., & Tao H. W. (2015). Sensory Cortical Control of a Visually Induced Arrest Behavior via Corticotectal Projections. *Neuron, 86*(3), 755-767. doi:10.1016/j.neuron.2015.03.048

Lo L., & Anderson D. J. (2011). A Cre-dependent, anterograde transsynaptic viral tracer for mapping output pathways of genetically marked neurons. *Neuron, 72*(6), 938-950. doi:10.1016/j.neuron.2011.12.002

Marcelja S. (1979). Initial processing of visual information within the retina and the LGN. *Biol. Cybern., 32*(4), 217-226. doi:10.1007/bf00337645

Mees L. M., Coulter M. M., Chrenek M. A., Motz C. T., Landis E. G., Boatright J. H., & Pardue M. T. (2019). Low-Intensity Exercise in Mice Is Sufficient to Protect Retinal Function During Light-Induced Retinal Degeneration. *Invest Ophthalmol Vis Sci, 60*(5), 1328-1335. doi:10.1167/iovs.18-25883

Milstein A. D., Bloss E. B., Apostolides P. F., Vaidya S. P., Dilly G. A., Zemelman B. V., & Magee J. C. (2015). Inhibitory Gating of Input Comparison in the CA1 Microcircuit. *Neuron, 87*(6), 1274-1289. doi:10.1016/j.neuron.2015.08.025

Mitamura T., Higashiyama S., Taniguchi N., Klagsbrun M., & Mekada E. (1995). Diphtheria toxin binds to the epidermal growth factor (EGF)-like domain of human heparin-binding EGF-like growth factor/diphtheria toxin receptor and inhibits specifically its mitogenic activity. *J. Biol. Chem., 270*(3), 1015-1019. doi:10.1074/jbc.270.3.1015

O'Sullivan M. L., Punal V. M., Kerstein P. C., Brzezinski J. A. t., Glaser T., Wright K. M., & Kay J. N. (2017). Astrocytes follow ganglion cell axons to establish an angiogenic template during retinal development. *Glia, 65*(10), 1697-1716. doi:10.1002/glia.23189

Pang J. J., & Wu S. M. (2011). Morphology and immunoreactivity of retrogradely double-labeled ganglion cells in the mouse retina. *Invest Ophthalmol Vis Sci, 52*(7), 4886-4896. doi:10.1167/iovs.10-5921

Peng Y.-F., Shi Y.-H., Ding Z.-B., Zhou J., Qiu S.-J., Hui B., Gu C., Yang H., Liu W.-R., & Fan J. (2013). α-Fetoprotein promoter-driven Cre/LoxP-switched RNA interference for hepatocellular carcinoma tissue-specific target therapy. *PLoS One, 8*(2), e53072. doi:10.1371/journal.pone.0053072

Ren C., Luan L., Wui-Man Lau B., Huang X., Yang J., Zhou Y., Wu X., Gao J., Pickard G. E., So K. F., & Pu M. (2013). Direct retino-raphe projection alters serotonergic tone and affective behavior. *Neuropsychopharmacology, 38*(7), 1163-1175. doi:10.1038/npp.2013.35

Rheaume B. A., Jereen A., Bolisetty M., Sajid M. S., Yang Y., Renna K., Sun L., Robson P., & Trakhtenberg E. F. (2018). Single cell transcriptome profiling of retinal ganglion cells identifies cellular subtypes. *Nat Commun, 9*(1), 2759. doi:10.1038/s41467-018-05134-3

Schiff W., Caviness J. A., & Gibson J. J. (1962). Persistent fear responses in rhesus monkeys to the optical stimulus of "looming". *Science, 136*(3520), 982-983. doi:10.1126/science.136.3520.982

Sernagor E., Eglen S. J., & Wong R. O. L. (2001). Development of retinal ganglion cell structure and function. *Prog. Retin. Eye Res., 20*(2), 139-174. doi:10.1016/s1350-9462(00)00024-0

Shang C., Liu A., Li D., Xie Z., Chen Z., Huang M., Li Y., Wang Y., Shen W. L., & Cao P. (2019). A subcortical excitatory circuit for sensory-triggered predatory hunting in mice. *Nat. Neurosci., 22*(6), 909-920. doi:10.1038/s41593-019-0405-4

Shang C., Liu Z., Chen Z., Shi Y., Wang Q., Liu S., Li D., & Cao P. (2015). BRAIN CIRCUITS. A parvalbumin-positive excitatory visual pathway to trigger fear responses in mice. *Science, 348*(6242), 1472-1477. doi:10.1126/science.aaa8694

Stegmeier F., Hu G., Rickles R. J., Hannon G. J., & Elledge S. J. (2005). A lentiviral microRNA-based system for single-copy polymerase II-regulated RNA interference in mammalian cells. *Proc. Natl. Acad. Sci. U.S.A., 102*(37), 13212-13217. doi:10.1073/pnas.0506306102

Su X., Tan Q. S., Parikh B. H., Tan A., Mehta M. N., Sia Wey Y., Tun S. B., Li L. J., Han X. Y., Wong T. Y., Hunziker W., Luu C. D., Owada Y., Barathi V. A., Zhang S. S., & Chaurasia S. S. (2016). Characterization of Fatty Acid Binding Protein 7 (FABP7) in the Murine Retina. *Invest Ophthalmol Vis Sci, 57*(7), 3397-3408. doi:10.1167/iovs.15-18542

Sun W., Li N., & He S. (2002). Large-scale morphological survey of mouse retinal ganglion cells. *J. Comp. Neurol., 451*(2), 115-126. doi:10.1002/cne.10323

Sylvester R., Haynes J. D., & Rees G. (2005). Saccades differentially modulate human LGN and V1 responses in the presence and absence of visual stimulation. *Curr Biol, 15*(1), 37-41. doi:10.1016/j.cub.2004.12.061

Taniguchi H., He M., Wu P., Kim S., Paik R., Sugino K., Kvitsiani D., Fu Y., Lu J., Lin Y., Miyoshi G., Shima Y., Fishell G., Nelson S. B., & Huang Z. J. (2011). A resource of Cre driver lines for genetic targeting of GABAergic neurons in cerebral cortex. *Neuron, 71*(6), 995-1013. doi:10.1016/j.neuron.2011.07.026

Wiener S. G., & Levine S. (1992). Behavioral and physiological responses of mother and infant squirrel monkeys to fearful stimuli. *Dev. Psychobiol., 25*(2), 127-136. doi:10.1002/dev.420250205

Yang K., & Ma H. (2011). Blockade of GABA(B) receptors facilitates evoked neurotransmitter release at spinal dorsal horn synapse. *Neuroscience, 193*, 411-420. doi:10.1016/j.neuroscience.2011.07.033

Yilmaz M., & Meister M. (2013). Rapid innate defensive responses of mice to looming visual stimuli. *Curr. Biol., 23*(20), 2011-2015. doi:10.1016/j.cub.2013.08.015

Yu B. C., Watt C. B., Lam D. M., & Fry K. R. (1988). GABAergic ganglion cells in the rabbit retina. *Brain Res., 439*(1-2), 376-382. doi:10.1016/0006-8993(88)91498-9

Zhang C., Kolodkin A. L., Wong R. O., & James R. E. (2017). Establishing Wiring Specificity in Visual System Circuits: From the Retina to the Brain. *Annu. Rev. Neurosci., 40*, 395-424. doi:10.1146/annurev-neuro-072116-031607

Zhao X., Liu M., & Cang J. (2014). Visual cortex modulates the magnitude but not the selectivity of looming-evoked responses in the superior colliculus of awake mice. *Neuron, 84*(1), 202-213. doi:10.1016/j.neuron.2014.08.037

Zhou Z., Liu X., Chen S., Zhang Z., Liu Y., Montardy Q., Tang Y., Wei P., Liu N., Li L., Song R., Lai J., He X., Chen C., Bi G., Feng G., Xu F., & Wang L. (2019). A VTA GABAergic Neural Circuit Mediates Visually Evoked Innate Defensive Responses. *Neuron*. doi:10.1016/j.neuron.2019.05.027

558 Supplementary information is available at *elife's* website.

559 **Supplemental Information**

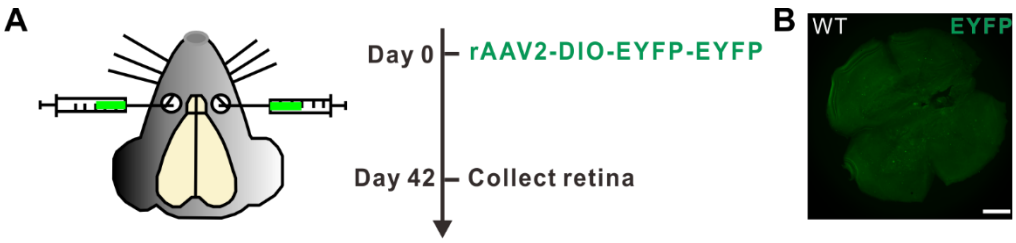

560 **Figure S1.** No virus-mediated labeling in control mice following *rAAV2-DIO-EYFP-*
561 *EYFP* infection. (**A**) Experimental strategy for viral delivery. (**B**) No EYFP-positive
562 cells are detected in the flat-mounted retina 42 days after virus infection, confirming
563 the Cre-depended EYFP expression in this study. Scale bar: 100 μm.

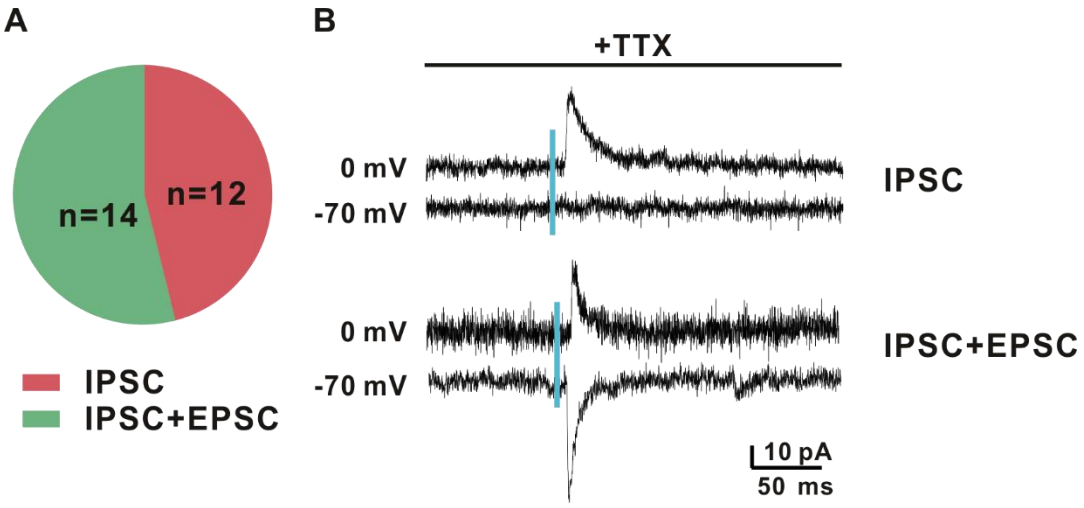

564 **Figure S2.** The properties of CHR2-induced currents. **(A)** IPSC-to-IPSC+EPSC ratios
565 for ChR2^{+} neurons are analyzed from *vGAT-Cre*/*Gad2-Cre* mice. (**B**) Example
566 averaged traces of ChR2-evoked IPSC (**upper**) and IPSC+EPSC (**lower**). IPSC:
567 ChR2 evoked excitatory (−70 mV), but no inhibitory (0 mV) currents in the presence
568 of TTX; IPSC+EPSC: ChR2-evoked excitatory (−70 mV) and inhibitory (0 mV)
569 currents in the presence of TTX.

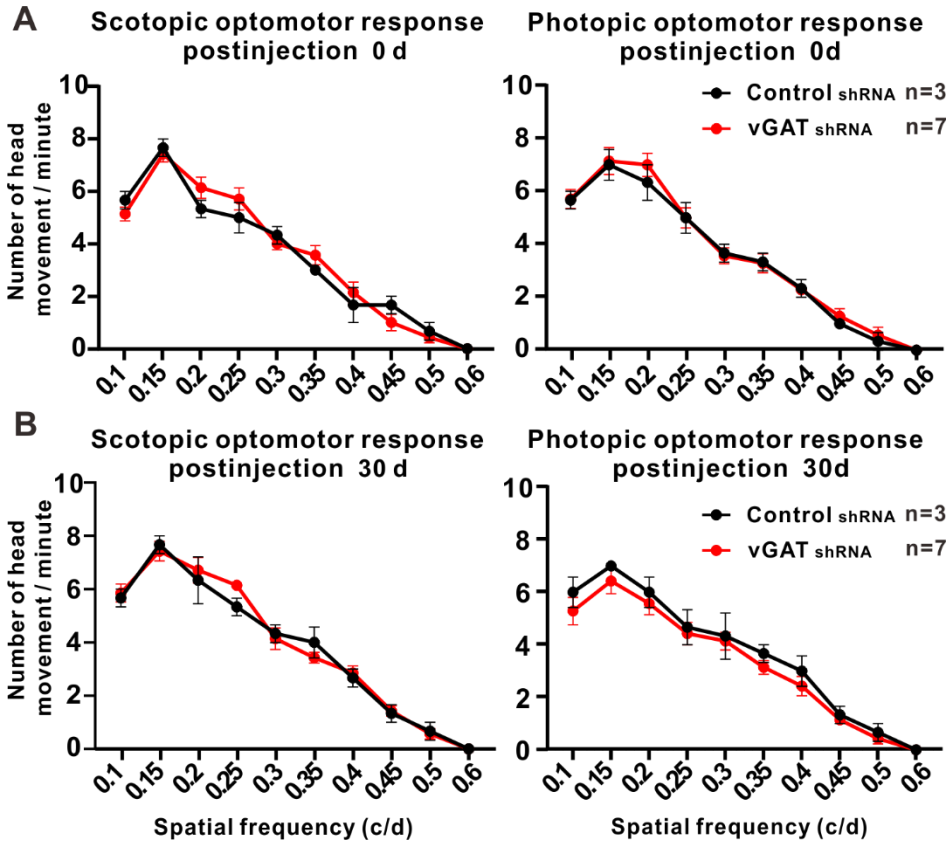

570 **Figure S3.** Functional release of GABA from spgRGCs are dispensable for the
571 optomotor response. **(A, B)** Before or 30 days after injection. there are no significant
572 differences on the optomotor response under scotopic and photopic conditions in the
573 Control shRNA or vGAT shRNA group.

574 **Supplemental Movie 1**

575 Example of looming-evoked defensive behavior in *Gad2-Cre* mice.

576 **Supplemental Movie 2**

577 Example of looming-evoked defensive behavior in *vGAT-Cre* mice.

578 **Supplemental Movie 3**

579 Effects of spgRGCs deletion on looming-evoked flight response in *Gad2-Cre* mice.

580 **Supplemental Movie 4**

581 Effects of spgRGCs deletion on looming-evoked flight response in *vGAT-Cre* mice.

Supplemental Movie 5

Example of looming-evoked defensive behavior in vGAT shRNA group.

Supplemental Movie 6

Example of looming-evoked defensive behavior in Control shRNA group.